REPORT DOCUMENTATION PAGE

Form Approved
OMB No. 0704-0188

1. REPORT DATE *(DD-MM-YYYY)*	2. REPORT TYPE	3. DATES COVERED *(From - To)*
	Technical Paper	

4. TITLE AND SUBTITLE

5a. CONTRACT NUMBER

5b. GRANT NUMBER

5c. PROGRAM ELEMENT NUMBER
62500F

6. AUTHOR(S)

5d. PROJECT NUMBER
2308

5e. TASK NUMBER
M4S7

5f. WORK UNIT NUMBER
345382

7. PERFORMING ORGANIZATION NAME(S) AND ADDRESS(ES)

8. PERFORMING ORGANIZATION REPORT

9. SPONSORING / MONITORING AGENCY NAME(S) AND ADDRESS(ES)

Air Force Research Laboratory (AFMC)
AFRL/PRS
5 Pollux Drive.
Edwards AFB CA 93524-7048

10. SPONSOR/MONITOR'S ACRONYM(S)
XC

11. SPONSOR/MONITOR'S NUMBER(S)

12. DISTRIBUTION / AVAILABILITY STATEMENT

Approved for public release; distribution unlimited.

13. SUPPLEMENTARY NOTES

See attached 8 papers, all with the information on this page.

14. ABSTRACT

15. SUBJECT TERMS

16. SECURITY CLASSIFICATION OF:			17. LIMITATION OF ABSTRACT	18. NUMBER OF PAGES	19a. NAME OF RESPONSIBLE PERSON
a. REPORT	b. ABSTRACT	c. THIS PAGE			Kenette Gfeller
Unclassified	Unclassified	Unclassified	A		19b. TELEPHONE NUMBER *(include area code)* (661) 275-5016

IEPC-95-18

LOW POWER ARCJET PERFORMANCE EVALUATION

Keith A. McFall*, Dennis L. Tilley*, and Frank S. Gulczinski III*
Phillips Laboratory
Edwards AFB, CA 93524

* Research Engineer, Electric Propulsion Laboratory

Abstract

The use of electric propulsion for stationkeeping and orbit repositioning missions offers significant advantages to Air Force users. Commercial interest in electric propulsion has largely focused on geostationary north-south stationkeeping of high power communication satellites, and has resulted in the development and flight qualification of several thruster types operating in the 1500-2000 W power range. Since the power available for propulsion on many current and future Air Force satellites is substantially less, the development of high performance low power thrusters is important to the support of Air Force missions. To support this development effort, the Air Force Phillips Laboratory has begun a low power arcjet research project to quantify and improve thruster performance. The objective of this effort is the improvement of thruster performance over the power range of 300-600 W using storable propellants. In this first phase, thrust, specific impulse, thrust efficiency and arcjet anode temperature were measured over the power range of 900 - 1200 W. A 1 kW modular arcjet operating on simulated hydrazine, N_2-$2H_2$, propellant with regular and extended length anodes was used for testing; the extended length anode provided a larger surface for temperature measurements. Thrust stand measurements were used to obtain arcjet performance data, and two-color optical pyrometry and thermocouple systems were used to measure anode temperature. Performance measurements were taken with both nozzles while temperature measurements were made with the extended anode alone. Measurement errors were quantified at 5% for thrust and 6-8% for temperature. Methods of reducing these errors to 2% for both cases are discussed.

Introduction

The high specific impulse (I_{sp}) of electric propulsion (EP) thrusters has made them attractive for large impulse on-orbit missions. For north-south stationkeeping (NSSK) applications, commercial communication satellite manufacturers began using 300 second specific impulse resistojets in the 1980's, introduced 500 second arcjets in 1993, and continue the development and qualification of higher performance EP thrusters. The evolution of these satellites has been to larger, higher power systems capable of providing up to 2000 W of electrical power for thruster operation. Many military and commercial satellites are not designed to provide this level of power for non-payload applications. The development of lower power arcjet thrusters provides a means of increasing thruster performance significantly beyond that of resistojets within the power constraints of these systems.

An example of a system requiring both higher thruster performance and reduced thruster operating power is the Defense Satellite Communications System (DSCS) III series satellites. The DSCS system program office initiated a satellite life extension program to examine the retrofitting of unlaunched DSCS III satellites. The objective was to increase operational life beyond the current 7 years. As part of this program, a NSSK propulsion system upgrade was studied. The study concluded that the use of electric propulsion would substantially increase satellite mission life due to reduced propellant usage rates. Both hydrazine resistojets and arcjets were identified as attractive alternatives to the existing hydrazine chemical thrusters. Resistojets were estimated at

increasing mission life from a current period of 7 years to 10 years, while a 500 second arcjet would increase life to 13 years. While the arcjet was the clear performance leader, arcjet technology at the 500 W power level had not reached a stage where it could be used for the DSCS III satellites due to the program schedule.

Recent sub-kilowatt arcjet studies [1,2] have reported performance figures that are significantly lower than those demonstrated for flight operational 1.8 kW and higher power arcjets [3,4]. Due to reduced Reynolds number, and potentially lower operating pressure, the fact that arcjet performance degrades as the power decreases is to be expected. The increases in viscous flow losses and frozen flow losses resulting from the change in size and operating pressure are anticipated mechanisms of performance decline. Power deposited in the anode is another energy loss mechanism. The decrease in volume to surface area associated with lower power arcjets is also expected to contribute to a reduction in thruster performance. Recent higher power (5-15 kW) hydrogen arcjet studies [5-7] have reported that increases in arc voltage, brought about through the use of non-conventional constrictor and nozzle designs, including regeneration, result in improved thruster performance. A contributing factor that has been identified has been a reduction in arc current and therefore resistive power deposition to the anode.

The objective of the low power arcjet research at Phillips Laboratory is the improvement of specific impulse and thrust efficiency of thrusters operating in the 300-600 W power range using storable propellants. The approach is to modify the arcjet anode design to decrease thermal and frozen flow losses. Anode temperature measurements will be made to determine radiative losses. The isolation and quantification of frozen flow loss effects will require the use of published numerical and experimental work in this area [8]. Performance effects will be confirmed with direct thruster performance measurements.

The results presented here represent the first stage of the performance improvement effort. Experiments were performed at the Electric Propulsion Laboratory located at the Phillips Laboratory, Edwards AFB, CA. Thrust, specific impulse, thrust efficiency and anode temperature were determined for a 1 kW class arcjet operating on simulated hydrazine, with a power range from 900 W to 1200 W. Thruster performance was determined using a thrust stand, and anode surface temperature measurements were made using optical pyrometer and thermocouple systems. Accuracy was estimated and methods for reducing measurement error were identified. With the system modifications identified, errors within 2% are anticipated for future thrust and temperature measurements.

Experimental Apparatus

I. Arcjet

For the work presented here, a 1 kW modular arcjet of NASA Lewis design was used (Figure 1).

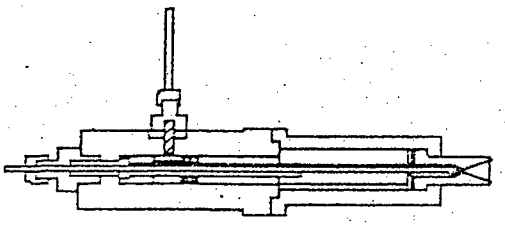

Figure 1: 1 kW Arcjet

The thruster was operated with two different anode inserts, shown in Figure 2, which differed in design only in the length of region upstream of the constrictor. The constrictor diameters, constrictor lengths, and expansion area ratios for both anodes were 0.635 mm, 0.254 mm, and 225, respectively. Upstream and downstream of the constrictor, the nozzle angles were 20° and 30° respectively.

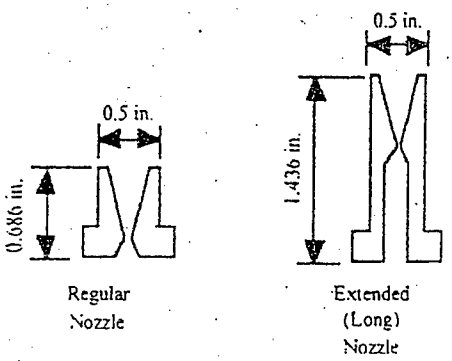

Figure 2: Arcjet Anode Inserts

The regular anode design is standard for the NASA arcjet. The extended anode was designed to allow for greater spatial resolution of temperature measurements, both optical and

thermocouple derived. The anodes were made of 2% thoriated tungsten. The anode housing was made of 316 SS (stainless steel). The use of stainless steel, due to its relatively low melting temperature, limited thruster operating conditions to specific powers not exceeding 28 MJ/kg for simulated hydrazine. A molybdenum anode housing will be used for future testing and should allow specific powers in excess of 50 MJ/kg.

II. Thrust stand

Arcjet thrust measurements were made using a displacement-type thrust stand. The arcjet is attached horizontally to an actively cooled inverted pendulum mount. Active cooling is also supplied to the top and front of the thrust stand, the regions exposed to the highest convective and radiative thermal fluxes. Cooling is used to minimize thermal stresses and reduce thermal drift. Arcjet thrust is calculated based on thruster displacement, which is calibrated using precise weights. Displacement is determined using two Lucas Schaevitz components: the Model 100-HR Linear Variable Differential Transducer (LVDT) is located within the thrust stand and generates a signal based on thruster displacement, Model DTR-451 Digital Transducer Controller (DTC), located outside of the test chamber, interprets the LVDT signal and provides both a digital readout and voltage output of the displacement. A minimum of 45 minutes was allowed for DTC warm up prior to data taking. The digital readout is used for manual displacement data taking and the voltage output is used for damping/oscillation control. Calibration of DTC output is accomplished using weights to simulate thruster operation. Three 5 gram masses, each with a tolerance within five milligrams, are sequentially loaded to the pendulum to displace the thruster amounts equal to 49.1 mN per mass for a total calibrated thrust of 147.2 mN.

Displacement of the thruster is proportional to thrust and inversely proportional to the effective spring constant of the pendulum system. The spring constant is contributed to by the power, propellant, and pendulum mount cooling flow lines that enter the device and are configured as spring coils used for retarding thruster displacement. The thrust stand was originally built for 10 kW arcjet operation. This configuration was felt to be too rigid - the DTC signal variations too small - for power levels of 1 kW and below. Propellant and power lines were replaced to increase thrust stand sensitivity.

The modified thrust stand provides a linear DTC signal response over the complete calibration range, and extends beyond the calibration range as well. This is demonstrated by the relatively small change, approximately 1-2%, in the slope of the DTC response curve when obtained during and after thruster operation. The thrust values shown in Figure 3 represent incremental increases in DTC signal due to thrust stand mass loading. These results demonstrate the extended range of thrust stand measurement linearity. Based on a nominal thrust of 200 mN, the linear response exceeds 350 mN.

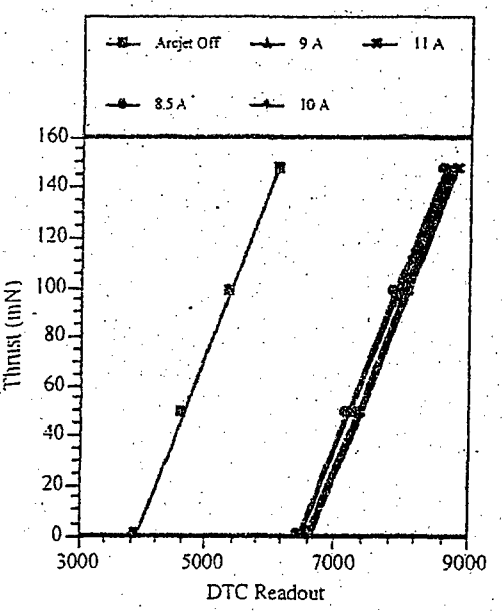

Figure 3: Thrust Stand Calibration Curves

III. Pyrometer and Thermocouples

Pyrometer

The two-color pyrometry system used in this study was manufactured by Vanzetti Systems (model 3003). Shown in Figure 4, The Vanzetti system is comprised of essentially three components: the fiber optic assembly, the detector, and a readout. The fiber optic assembly consists of a lens cell, which focuses thermal radiation from the target into two fiber optic cables linked to the detector. Four fiber optic assemblies were available for use, each with a different target distance and spot size. The fiber used in this study had a target distance of 45.7 cm (18 in.) and a 1.8 mm (0.072 in.) spot size. A third fiber optic cable is used to back-light the target for alignment purposes (using a Vanzetti LS1-1 light source).

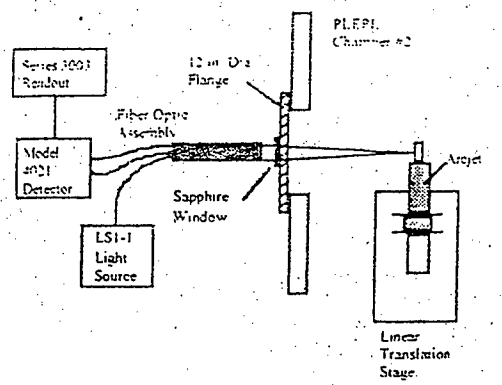

Figure 4: Optical Pyrometry Setup

The detector housing (Vanzetti model 4021) consists of two PbS photodetectors filtered with slightly different bandpass filters (nominally 1.5 and 2.25 μm). The photodetectors are thermally compensated, and radiation to them is chopped at 400 Hz. The electrical signals from the photodetectors are routed to the Vanzetti model 3003 readout, which performs further electronic processing, and also has a digital display of the gray-body temperature and various preprocessed voltages. With the optics fixed, the target spot location was varied using a 100,000 counts/cm linear translation stage to move the arcjet in the axial direction. Thermal radiation from the target also passed through a sapphire window at the vacuum chamber interface. The effect of the sapphire window on the measurements was negligible because it has non-varying transmission characteristics over the bandwidths of both filters. This assumption was also verified experimentally using a blackbody source.

Thermocouple

For contact measurement of anode temperature, type-C (W-5% Re, W-26% Re) were used. The thermocouple setup was tested and verified for accuracy using a blackbody cavity over a temperature range from 900-1200 C.

IV. Propellant System

Propellant flow for the arcjet was regulated through MKS Type 1162B Mass Flow Controllers. The nitrogen controller had a maximum flow rate of 10,000 standard cubic centimeters per minute (SCCM) and the hydrogen controller had a maximum rate of 30,000 SCCM. Argon used for starting the arcjet was supplied through a bypass line that was regulated by a needle valve calibrated against the nitrogen flow controller. The manufacturers' specifications for these controllers indicate an accuracy of ± 1.0% of full scale and a repeatability of ± 0.2%. An independent confirmation of accuracy was desired and a calibration system was constructed. This system consisted of a MKS Baratron® Type 122B Absolute Pressure Gauge, a Jenco Model 701 Type J Thermocouple Thermometer, and a 3.83 liter plenum. The system is shown in Figure 5. Using the Ideal Gas Law and the relation between mass flow rate and number density, it was possible to determine a relationship between pressure and mass flow rate:

$$\frac{P(t)VM_W}{R_U T(t)} = \dot{m}t \qquad (1)$$

Where:

P(t): Pressure in plenum
V: Volume of plenum
M_W: Molecular Weight of Gas
R_U: Universal Gas Constant
T(t): Temperature in plenum
$\dot{m}$: Mass Flow Rate
t: Time

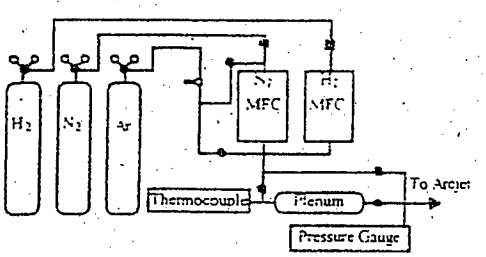

Figure 5: Mass Flow System

The slope of a plot of the left hand side of the equation versus time is equal to the mass flow rate. This rate was then compared to the rate set on the MKS flow controller. The full scale errors determined for this analysis are shown in Figures 6 and 7.

These calibrations indicate errors ranging up to 4% of full scale reading for nitrogen and -1.3% for hydrogen. The discrepancy between these results and the manufacturers' specifications is not fully understood at this time but is believed to originate from errors in our calibration procedure. However, the error in the flow regimes used in this study were of the order of ± 1%. This corresponds to a mass flow error of approximately 5% at a nominal nitrogen flow rate of 2000 SCCM.

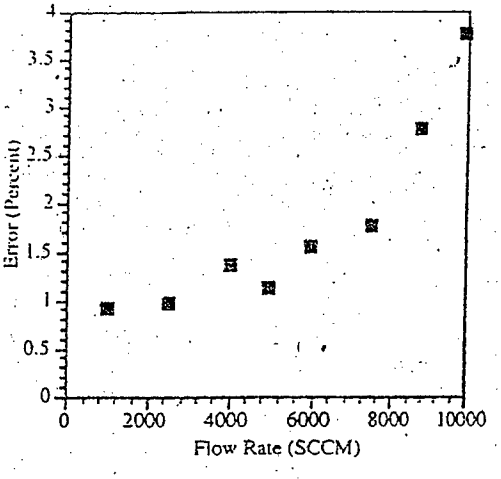

Figure 6: Full Scale Error vs. Flow Rate: Nitrogen Flow Controller

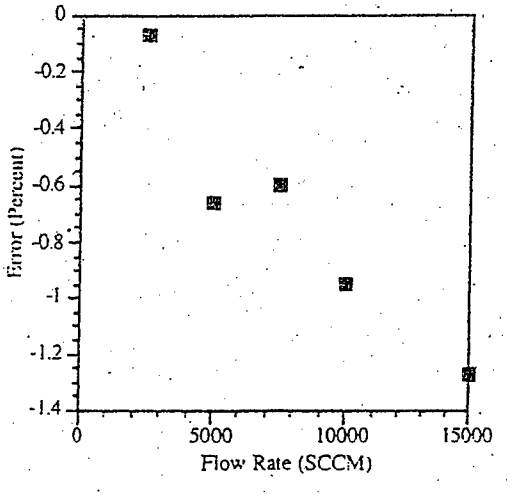

Figure 7: Full Scale Error vs. Flow Rate: Hydrogen Flow Controller

V. Power System

The purpose of the power system is to provide a means of initiating arcjet propellant breakdown, transitioning to an arc discharge, and establishing steady state thruster operation. The system consists of a main power supply bank and a supplementary power supply used during arcjet breakdown and arc transition. The former is regulated and capable of 350 V at 35 A. The later is unregulated with a 375 V open circuit voltage and a 4 A short circuit current. The power system is configured so that the unregulated supply is passively switched out of the circuit when it is turned off. This is needed since the unregulated supply is not designed for continuous operation above 4 A. Switching is accomplished by placing a diode across the unregulated supply leads so that it is negatively biased when the supply is on (Figure 8). As soon as the unregulated supply is turned off, the diode becomes positively biased relative to the rectifying diodes inside the supply, and conduction occurs. A 5.4 ohm ballast resistor is place in series with the arcjet and is necessary for stable arcjet operation due to the relatively slow response time of the power supplies.

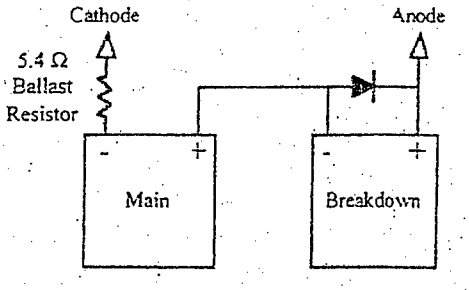

Figure 8: Power Supply Switching Setup

The arcjet startup procedure used for simulated hydrazine operation begins with the arcjet flow set at approximately 100 mg/s of argon. The main power supply is set to approximately 250 V with a current limit at 10 A. Arcjet breakdown is initiated when the unregulated supply is turned on. High mode operation occurs almost without exception, though low mode operation can occur more frequently at lower mass flow rates; it is also sometimes indicative of small deposit buildups, thought to result from grafoil seal decay, in the upstream region of the nozzle. For the transition to simulated hydrazine, the argon mass flow was reduced to about 60 mg/s. The reduced argon mass flow resulted in a more rapid transition to the other propellants. The nitrogen and hydrogen flow controllers were set to their respective flow levels and turned on to initiate propellant flow. After five seconds to allow for flow rate stabilization, the argon flow valve was shut. Within thirty seconds, the operating voltage rises, stabilizes briefly, rises more, then falls to a steady-state value.

Voltage measurements were made at the test chamber power feedthough. A precision resistor voltage divider is connected to a panel readout with 1 volt accuracy. Current is measured using the digital current readout from the main power supply and is accurate to 0.01 A.

VI. Test Chambers and Vacuum System

Thrust and anode temperature measurements were performed in test chambers number 1 and 2, respectively. Chamber number 1 is 1.8 m in diameter, 2.4 m in length and constructed of stainless steel. The thrust stand is mounted to a cantilever structure attached to the chamber door. The structure is partially supported by two 0.5" steel rods, shown in Figure 9; the reflective tape surrounding the rods was used in an attempt to reduce thrust stand thermal drift. The pressure within chamber number 1 was monitored with a Varian model 531 thermocouple gauge with a Varian model 801 thermocouple gauge controller. Chamber number 2 is 2.4 m in diameter, 3.7 m in length and constructed of mild steel. Optical and thermocouple measurements were made through a 12" flange with multiple feedthroughs, shown in Figure 10. The pressure within chamber 2 was monitored with a MKS Baratron® model 122BA.

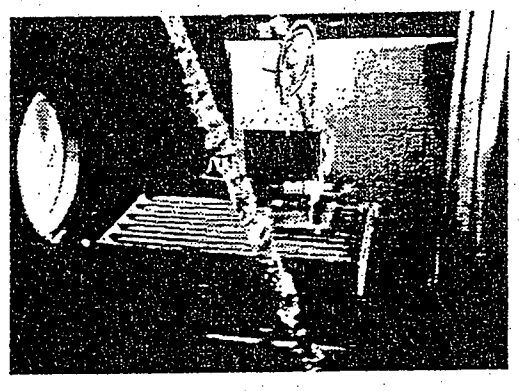

Figure 9: Arcjet Support Structure

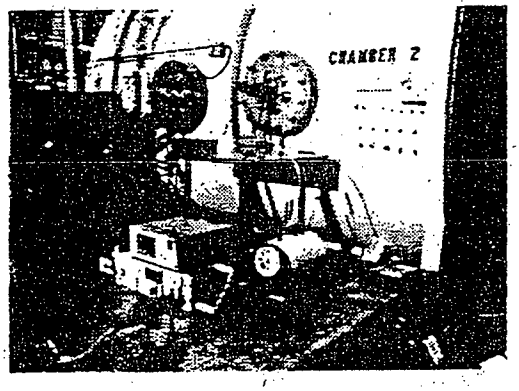

Figure 10: Optical/Thermocouple Feedthrough

Both chambers were supported by a common vacuum system composed of two pump trains capable of a total volumetric flow of 11000 liters/sec (23000 CFM). Only one chamber was operated at a time, the other being isolated by gate valves. The pressure obtained for chamber number 1 with no propellant flow was 30-40 mtorr. For chamber number 2, the value was 60-70 mtorr.

Results and Discussion

I. Thrust Stand Measurements

Thrust stand measurements made during this first phase of the Phillips Laboratory sub-kilowatt performance improvement effort were used to evaluate thrust stand accuracy, examine the performance differences between the regular and extended length anodes, and establish 1-kW-level performance baselines for future lower power testing.

Accuracy was examined from the standpoint of linear response to calibration mass loading, the instantaneous effect of thruster operation, and the magnitude of thermal drift. Linear response was evaluated by calculating the best linear fit of the four calibration data points relating DTC output to mass loading and determining the maximum error from this line; this error is estimated at 0.5%. The instantaneous effect of thruster operation was evaluated based on the change in slope of the calibration curve before, during, and after thruster operation; this error is estimated at 1-2% when post run calibration are made and 0.2-0.4% when calibrations are made prior to thruster operation. It should be noted that calibrations taken prior to thruster operation will only be accurate if thermal drift is minimal. Thermal drift was measured using DTC output changes during steady state thruster operation. Hydrazine arcjet operation at a specific power of 22 MJ/kg resulted in a drift rate of approximately 3% over thirty minutes of thruster operation. The arcjet was operated over a period of two hours with drift measurements being taken after 30 minutes, to allow for thruster thermalization. This drift rate was seen to change in magnitude with thruster operating conditions. While performance data for hydrogen arcjet operation will not be presented, thermal drift measurements were also made using hydrogen at a specific power of 60 MJ/kg. The arcjet was seen to operate visibly cooler and the absolute drift rate was about half that of the hydrazine case. However, since the thrust level was also about half that of the hydrazine case, the relative drift was still approximately 3% over 30 minutes. Attempts were made to reduce thermal drift by radiatively insulating the thrust stand cantilever support rods, but the improvements seemed

minimal. A conservative figure for thrust stand accuracy is taken to be 5%.

Based on the examination of error mechanisms discussed above, it was decided to limit thruster operation between calibrations to approximately 30 minutes. The procedure is as follows. The thruster was started on argon propellant, transitioned to simulated hydrazine, and run for 30 minutes prior to recording thrust measurements. Two to three minutes of operation time was allowed between current and mass flow set points. The plenum pressure and thruster voltage were monitored to assure steady state operation. The thrust stand oscillator/damper was switched to oscillate for 2-3 seconds then returned to damp prior to each recording of thrust.

1-kW class arcjet performance was measured for simulated hydrazine propellant. Thrust and mass flow measurements were used to determine specific impulse and thrust efficiency; no correction was made for initial flow enthalpy in the thrust efficiency calculation. The cathode gap was set at 0.6 ± 0.013 mm. Performance measurements for simulated hydrazine are presented at mass flow rates of 50.0, 45.2, and 40.5 mg/s and a current range from 8.5 to 11 A. The chamber pressure during operation was between 50 and 70 mtorr.

Voltage-Current data are presented in Figure 11. The voltage difference between the regular and extended length anode cases is felt to be more a function of arcjet gap variations than a result of design difference; under the same operating conditions, a variance in voltage of up to 7 V was seen when the cathode gap position was reset to the same position.

Thrust-Power data are presented in Figure 12. Thrust levels for the extended anode are shown to be up to 5% greater than corresponding regular nozzle cases. The difference is potentially due to the reduced thermal losses to the main body of the arcjet, but it is also within thrust stand and mass flow measurement errors.

Specific impulse-specific power data are presented in Figure 13. As with thrust measurements, the specific impulse levels for the extended anode are uniformly higher than for the regular nozzle. The explanation for this is thought to be the same as for thrust.

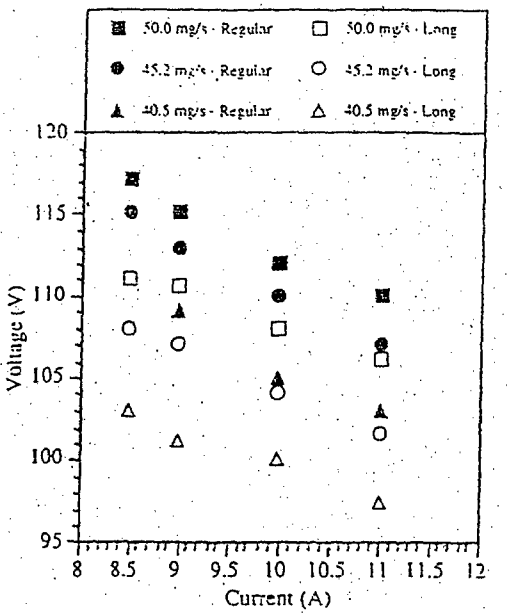

Figure 11: Voltage-Current Measurements

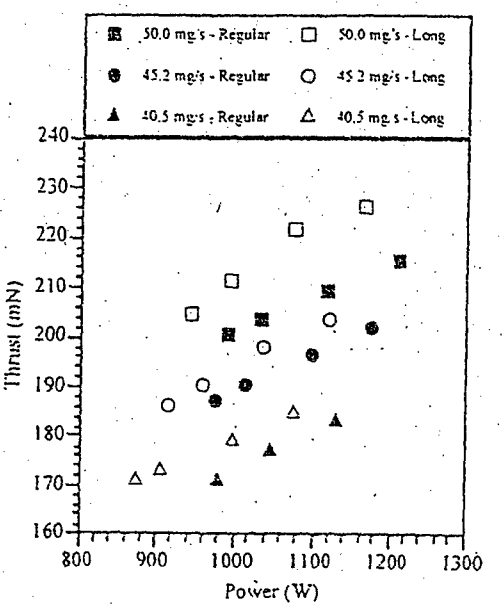

Figure 12: Thrust versus Arcjet Power

Thrust efficiency-specific power data are presented in Figure 14. The decrease in efficiency with increasing specific power, that is evident from most of the data, is expected due to increasing thermal, frozen flow, and viscous losses as the arcjet is operated hotter and the propellant temperature increases. The extended anode data at the 50.0 mg/s mass flow does not exhibit this trend. It is felt that measurement error explains

this unexpected, though relatively small, deviation.

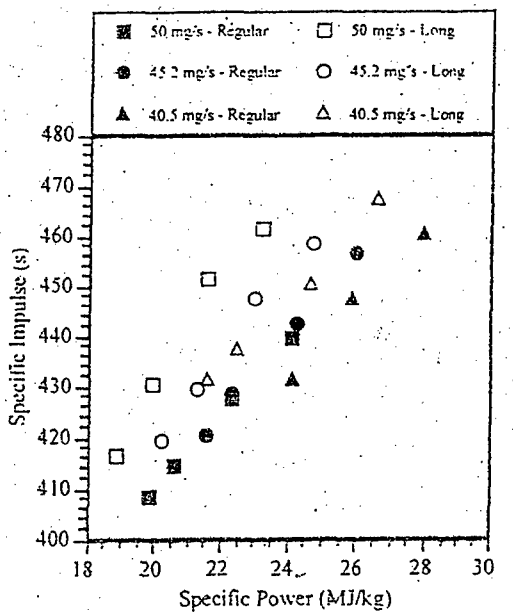

Figure 13: Specific Impulse versus Specific Power

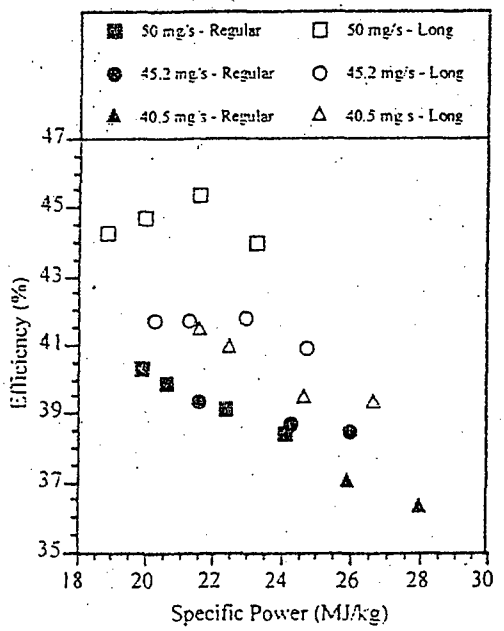

Figure 14: Specific Power-Efficiency Measurements

Assuming a thrust measurement error of 5% and a mass flow error of 5%, worst case estimates of thruster overall measurement error, based on worst case combinations of thrust stand and mass flow error is estimated at: 5% for thrust, 10% for specific impulse, and 15% for thrust efficiency. These errors should be able to be reduced substantially by reducing thermal drift and operating flow controllers near full scale flow. Thermal drift will be addressed through improved support structure insulation and , if necessary, thrust stand mounting modifications. A reduction in thrust stand error to 1-2% is anticipated based with the near removal of most thermal drift effects. With the use of a separate set of flow controllers for sub-kW operation, the full scale flow will be reduced by one order of magnitude. This will reduce the mass flow error to 1-2% over a power range of 300-600 W.

II. Anode Temperature

The motivations for these measurements are two-fold. First, comparisons of measured temperature distributions to those predicted by arcjet flow models [9,10] can be used to evaluate such models, and to investigate arc attachment and anode power deposition mechanisms. Second, low power arcjet studies indicate that the anode power fraction increases as power decreases [11], suggesting that thermal losses are important in arcjets which operate at ~500W and below. Anode temperature measurements can be used to characterize these losses, and spatially-resolved data on 1-kW class arcjets is relatively scarce.

In this section, preliminary outer anode body temperature measurements are presented. Two temperature measurement approaches were investigated: thermocouple techniques and optical pyrometry. To facilitate such measurements, the standard arcjet configuration was refitted with an extended anode such that outer temperature measurements could be obtained in the converging, constrictor, and diverging sections of the nozzle. All experiments were performed in chamber 2 of the PL Electric Propulsion Laboratory, described in detail elsewhere [12]. The chamber pressure during arcjet operation was approximately 120 mtorr for all tests presented in this section.

Optical Pyrometry

The two-color pyrometry system used in this study was manufactured by Vanzetti Systems (model 3003). Although not originally designed for this application, equipment limitations dictated the adaptation of this system to obtain low power arcjet temperatures. Its basic principle of operation is to ratio the radiation

intensity from a hot source at two slightly different wavelengths to determine the surface temperature independent of emissivity, [13]. Two-color pyrometry is based on the assumption that the emissivity at the two wavelengths are equal, or sometimes on a less restrictive assumption that the ratio of the two emissivities is temperature-insensitive. Unfortunately, neither of these assumptions applied to tungsten at the wavelengths sampled. For this reason, the raw signals from the detector were corrected to obtain accurate temperatures using a method described below.

The following correction method was used to adjust measurements made by the Vanzetti system to our application:

$$\frac{V_B}{V_A} = G_0 \frac{t_w(\lambda_B)}{t_w(\lambda_A)} \frac{\varepsilon(\lambda_B,T)}{\varepsilon(\lambda_A,T)} \exp\left(f\frac{hc}{kT}\left(\frac{1}{\lambda_A}-\frac{1}{\lambda_B}\right)\right) \quad (2)$$

Where:

V_A: Voltage of Detector A
λ_A: Center-Wavelength of Filter A
V_B: Voltage of Detector B
λ_B: Center-Wavelength of Filter B
h: Planck's Constant
k: Boltzman Constant
c: Speed of Light
T: Temperature
$\varepsilon(\lambda,T)$: Spectral Emissivity of Tungsten
$t_w(\lambda)$: Sapphire Window Transmittance

G_0 accounts for many factors such as the gain settings in the electronics, the response of the PbS detectors, and the transmission characteristics of the filter and fiber optics. f is a factor to account for the fact that there is actually a bandwidth associated with λ_B and λ_A (2.01-2.47 μm for A, and 1.20-1.90 μm for B). G_0 and f are obtained by calibrating the pyrometry system using a blackbody source, and emissivities of tungsten are obtain from the literature [14]. Once G_0 and f are obtained, V_B/V_A is measured at each axial location along the anode, and equation 2 is used to calculate T (using iteration).

It is estimated that two sources of error dominate the uncertainty associated with these measurements and the correction scheme. The first is the use of empirically determined emissivity values. Although, researchers can measure with high accuracy (~1%) the emissivity of a tungsten surface, 20% variation among different research groups is not uncommon [14]. Assuming that these differences are due to surface effects (such as oxidation), and because the surface state of the arcjet anode is unknown, suggests that this source of error non-negligible. The second source of error is the use of a non-weighted average of the emissivity over the filter bandwidth in equation 2. This error could be eliminated by integrating the emissivity over the blackbody distribution, the response of the detector, and the transmittance of the filter and fiber optics. This was not performed due to the lack of information on some of these quantities. The sensitivity of the measurements to these two sources of error will be briefly discussed later. Clearly, more investigation is required to better quantify the accuracy of these measurements.

Using $t_w(\lambda_B)/t_w(\lambda_A)$=0.989, and a non-weighted average of the emissivity data from reference 14, the following expressions were obtained for ε_A and ε_B:

$$\varepsilon_A = 0.0751 + 5.294\text{x}10^{-5}T \quad (3)$$

$$\varepsilon_B = 0.2165 + 2.592\text{x}10^{-5}T \quad (4)$$

for:

$$1200\ K \le T \le 2200\ K$$

Note that the above expressions were obtained from line-fitting the average emissivity as a function of temperature, which was linear over the relevant temperature range for this experiment.

Three separate calibration processes were performed to obtain and verify the values of G_0 and f. In addition, a calibration method using a thermocouple placed on a tungsten target was performed to verify the above correction scheme. More will be discussed on this in the next section. A factory calibration of the entire system was performed at Vanzetti Systems (i.e. to obtain a V_B/V_A versus T curve) for each of the fiber optic assemblies. In addition, before each test run the system was calibrated using a Vanzetti calibration lamp (model CS1A). For a given lamp setting, the gain on each detector signal was adjusted as per factory calibration. Finally, a Graseby Infrared blackbody radiation source (model 564), along with a model IR-201 temperature controller was used to independently validate the factory calibration for temperatures 1200 °C and below. All methods were found to be consistent with each other. Properly calibrated, the accuracy of the Vanzetti two-color pyrometer for a gray-body target is ~1%.

Figure 15 shows typical results of measurements obtained with the long-nozzle arcjet operating on a hydrazine-type mixture at power levels between 1 and 1.2 kW. Peak temperatures are located on the downstream tip of the anode, and are in the 1400-1600K range. The magnitude of these temperature measurements are about 200K higher than single-point measurements taken on other arcjet configurations [15-18]. The likely cause of this discrepancy is the comparative size of the long-nozzle arcjet diameter, which is more than 2x smaller than the nozzle diameters used in previous studies [15-18].

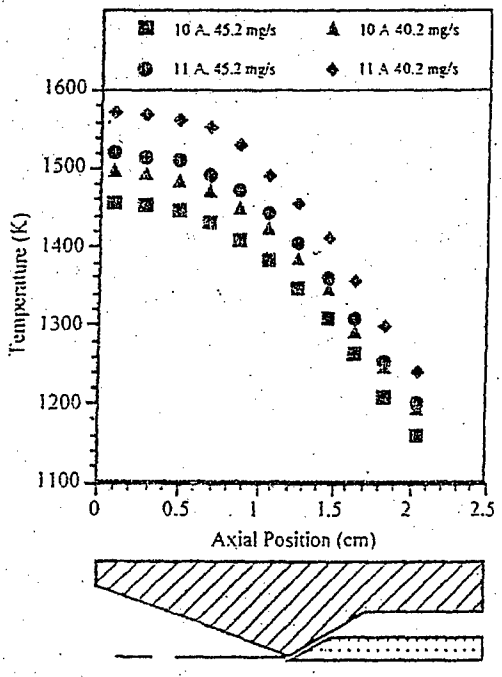

Figure 15: Typical Arcjet Anode Temperatures (With Anode)

The trends in temperature versus power and mass flow rate also match those from previous studies. Future work will focus on the direct comparison of measured temperature profiles with those predicted by models [9-10].

To investigate the sensitivity of temperature measurements calculated using equation 2 to the emissivity ratio, the ratio was increased and decreased by its approximate uncertainty (10%). Figure 16 shows the sensitivity of the temperature profiles to the emissivity ratio. A lower emissivity ratio corresponds to higher indicated temperature. The uncertainty in temperature is ~100K or about 6-8%.

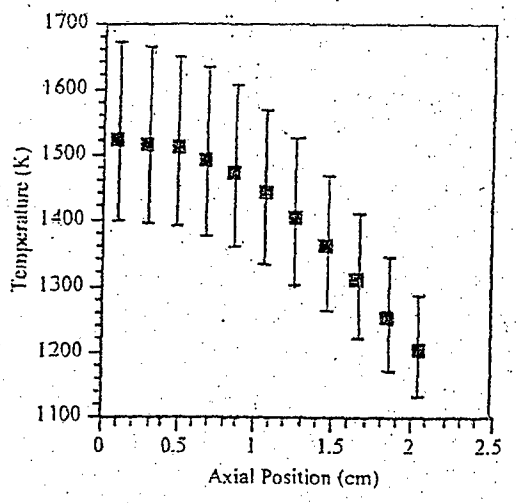

Figure 16: Uncertainty Associated with Anode Temperature Measurements

Thermocouples

Practically all arcjet anode temperature measurements using thermocouples have utilized the K-type [15-18]. This is due to the ease of attachment to the anode via spot welding, although their maximum operating temperature is 1650K. For our first attempt to implement this technique, we chose to use the type-C (W-5% Re, W-26% Re) thermocouple (TC), due to the high temperature at the anode tip (the maximum operating temperature of a type-C TC is 2590K). To avoid the use of welding techniques, such that the anode can be removed from the forebody of the arcjet, other attachment techniques were investigated. However, these methods proved to be troublesome.

In one attempt, the TC was attached to the anode by the use of 0.254 mm diameter (10 mil) tungsten wire, with the leads up to the TC bead (1.3 mm diameter) insulated with small alumina tubing (1.6 mm OD). Although the TC was firmly attached to the anode, two problems were readily evident. First, the presence of the small TC and tungsten wire provided enough additional radiating area to significantly perturb the temperature at the anode. Figure 17 illustrates this effect, with the anode temperature altered by as much as 100K. The second problem was that the thermocouple indicated a temperature that was about 200K lower than that of the pyrometer. This discrepancy is due to the high thermal contact resistance between the TC bead and the anode; and as described above, due to the additional radiating area of the bead.

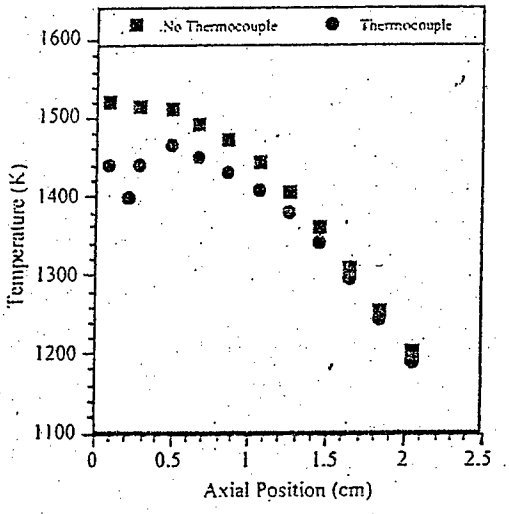

Figure 17: The Effect of the TC Attachment at 0.2 cm on Arcjet Anode Temperature

Another attachment method used a strip of thin tungsten foil (4 mm width, 0.05 mm thick) to create an enclosure around the TC bead (0.6 mm diameter.). The foil and TC bead were again attached using 0.254 mm diameter tungsten wire, wrapped on both sides of the TC bead, around the anode and along the strip of tungsten foil. This attachment method created a closed blackbody cavity around the TC bead, thus ensuring sufficient radiative contact with the arcjet anode and tungsten foil. Again this method perturbed the temperature profile along the anode, but also provided a means of comparison with the pyrometer, which was focused on the tungsten foil. Shown in Table 1 is this comparison.

Arcjet Current (A)	Mass Flow Rate (mg/s)	Pyrometer Temp. (K)	Thermocouple Temp. (K)
10	40	1239 +90/-78	1347
11	40	1279 +97/-83	1394
11	45	1253 +93/-78	1366

Table 1: Comparison of pyrometer and thermocouple temperature measurements on a tungsten foil wrapped around the arcjet anode.

The pyrometer measurements are about 100K lower than those obtained by the thermocouple, although this discrepancy would be reduced considerably by using properly weighted emissivities in equation 2. Weighting the emissivity with the blackbody distribution only significantly narrows the differences between the pyrometer and thermocouple.

Improved Techniques

We are now examining other thermocouple attachment techniques and possibly the welding of alternative TCs to the anode body. Further work is required to verify the pyrometry measurements, and to investigate other issues such as the effect of vacuum chamber pressure on the temperature distributions. For high precision measurements (~2% error), a system using single color pyrometry while imaging the entire arcjet anode will be investigated[19].

Conclusions

Arcjet performance and temperature measurements were performed as part of a Phillips Laboratory low power arcjet research effort. Thrust stand, optical pyrometry and thermocouple measurements were made on a 1-kW class arcjet operating over a 900-1200 W power range using simulated hydrazine as a propellant. Current measurement errors were estimated at 5% for thrust, 10% for specific impulse, 15% for thrust efficiency, and 6-8% for temperature. Primary sources of performance error were identified as thrust stand thermal drift and inherent mass flow controller error. These errors can be reduced to within 2% by improving thrust stand thermal isolation and using mass flow controllers with full range settings near the required flow settings. Temperature measurement error is related to the selection of optical pyrometer equipment and thermocouple selection/joining techniques. The present optical pyrometer uses a two color system that would be excellent for gray-body temperature measurements. Tungsten emissivity varies greatly with both temperature and wavelength and therefore requires detailed corrections to be made on the two-color pyrometery data; a single color pyrometer system is being considered to address this measurement error and reduce it to 2%. Thermocouple error can be reduced by improved attachment methods and thermocouple type selection. Further evaluation will be required to determine the level of error reduction.

Subsequent work will focus on the improvement of thruster performance through reductions in thermal losses and frozen flow losses. Anode design changes focusing on improved regenerative transport, propellant thermalization,

and refractory material selection will be made. Thrust stand measurements will be used to quantify performance changes. The anticipated reduction in thrust, mass flow, and temperature error to within 2% for a hydrazine thruster operating in the power range from 300-600 W will be necessary for this effort.

Acknowledgments

The authors wish to acknowledge the following individuals for assistance on this project: David White (Sparta, Inc.) for instrumentation and power system support; Keith Lawson and John Shoemaker (PL/TOFS) for test apparatus fabrication; Jeffrey Pobst (Hughes STX) for arcjet operations support; Michael Alfono (PL/HSAP) for experiment support; Lee Johnson (Aerospace Corporation) for arcjet design support; David Rice and Tom Andrews (JPL) for arcjet fabrication support; Dr. Graeme Aston for arcjet operation suggestions.

References

1. Sankovic, J.M. and Jacobson, D.T., "Performance of a Miniaturized Arcjet", AIAA Paper No. 95-2822, 1995.

2. Deininger, W.D., et al, "Comparison of Low Power Arcjet Operation ATBPD and Centrospazio", AIAA Paper No. 92-3115, 1992.

3. Smith, R.D., et al, "Flight Qualification of a 1.8 kW Hydrazine Arcjet System", IEPC Paper No. 93-007, 1993.

4. McLean, C.H., Lichan, P., Sankovic, J., "Life Demonstration of a 600-Second Mission Average Arcjet", AIAA Paper No. 94-2866, 1994.

5. Hoskins, W. A., et al, "A Comparison of Regenerative and Conventional Arcjet Performance", AIAA Paper No. 94-3124, 1994.

6. Aston, G., Kolts, J., Aston, M., "5 - 15 kW High Performance Hydrogen and Ammonia Arcjets", AIAA Paper No. 94-2871, 1994.

7. Riehle, M., Kurtz, H., Auweter-Kurtz, M., "Performance Investigation of Radiation and Regeneratively Cooled 5 kW Thermal Arcjet Thruster", AIAA Paper No. 94-3123, 1994.

8. Butler, G.W., Boyd, I.D., Cappelli, M.A., "Non-Equilibrium Flow Phenomena in Low Power Hydrogen Arcjets", AIAA Paper No. 95-2819, 1995.

9. Butler, G.W., Kull, A.E., King, D.Q., "Single Fluid Simulations of Low Power Hydrogen Arcjets", AIAA Paper No. 94-2870, 1994.

10. Krier, H. and Burton, R.L., "Two Temperature Modeling of Multicomponent Arcjets with Experimental Validation", Proc. of the 1995 AFOSR Contractors Meeting, Chicago, IL, 1995, pp. 83-86.

11. Sankovic, J.M. and Curran, F.M., "Arcjet Thermal Characteristics", AIAA Paper No. 91-2456, 1991.

12. Johnson, L.K., et al., "Frequency-domain Electromagnetic Characteristics of a 26 kW Ammonia Arcjet", AIAA Paper No. 93-2393, 1993.

13. Quinn, T.J., *Temperature*, Academic Press, Inc., 1983.

14. Gubareff, G.G., Janssen, J.E., Torborg, R.H., *Thermal Radiation Properties Survey*, 2nd edition, Honeywell Research Center, Minneapolis, MN, 1960.

15. Morren, W.E., "Low-Power Arcjet Test Facility Impacts", AIAA Paper No. 92-3532, 1992.

16. Yoshikawa, T., et al., "High Performance DC Arcjet Thruster for 1 kW System Definition", AIAA Paper No. 94-3004, 1994.

17. Cruciani, G., et al., "Advanced Laboratory Model, 1-kW Class Arcjet Engine Testing", IEPC Paper No. 91-044, 1991.

18. Yamada, T., et al., "Thermal Analysis and Thrust Performance of a Low Power Arcjet Thruster", AIAA Paper No. 90-2581, 1990.

19. Hoskins, W.A., et al., "Measurement of Energy Deposition Modes in an Intermediate Power Hydrogen Arcjet", IEPC Paper No. 93-216, 1993.